Sixth International Symposium on Marine Propulsors
smp'19, Rome, Italy, May 2019

A computational analysis of a marine propeller with tubercle and its contribution in reducing sheet cavitation.

Nicolas Charalambous[1], **Ian Eames**[1]

[1] Department of Mechanical Engineering, University College London, Torrington Place, London, UK

ABSTRACT

The paper examines the influence of wavy leading edges (tubercles) for a modified propeller in relation to the cavitation formation. Cavitation is the main source for the radiation of underwater noise. The leading edge of the marine propeller DTMB 4119 has been modified using OpenProp and compared with the DTMB 4119 propeller under the same operational conditions and the same cavitation number. The computational studies have been performed using a RANS solver with a multiphase mixture flow model applying the Schnerr-Sauer cavitation model in order to resolve the cavitation structures in the propeller. The results showed that the influence of the tubercles to the cavitation inception and formation can contribute to controlling the generation of sheet cavitation to the propeller surface and the opposite sign vorticity generated downstream of the propeller can locally influence the flow passing the surface of the propeller resulting to a modified flow environment that can interact with the mechanism responsible to the formation of sheet cavitation.

Keywords

Cavitation, Tubercles, CFD, vorticity, Cavitation model

1 INTRODUCTION

Underwater radiated noise has significantly increased during the last two decades. The reason for this is the increase in the volume of shipping and the growth in the international trade. This has resulted in larger ship sizes of the main ship types (Bulk carriers, Tankers, Container ships) and furthermore, to the increase of speed for some types of ships. Underwater noise has been found to have adverse effects to marine mammals since it can interfere with several aspects of their life especially in areas with increased vessel traffic density. In 2014 IMO has produced guidelines in order to mitigate underwater noise, however the problem still remains and in some areas is even becoming worst. One of the major sources of URN is the propeller and especially when it is cavitating. As a result the need to further investigate improved propeller designs and also novel design features is becoming a necessity. Furthermore the use of reliable computational predictions tools for capturing cavitation phenomena is also important since it will help the improvement of existing designs and the generation of new propeller designs. The aim of this paper is to describe the cavitation formation for a wavy leading edge and furthermore, to apply this formation to a marine propeller to analyse the performance with cavitation in contrast to a propeller without tubercles. Hydrofoils with tubercles have been studied both computationally and experimentally, the majority of the research focused on the performance of these hydrofoils and their effect on the lift to drag ratio. It was found that these hydrofoils can perform at their best at angle of attacks that are beyond the stall angle for hydrofoils and are exceeding 20^o. This characteristic of the hydrofoils with tubercles has been identified by Watts & Fish (2001), Miklosovic et al. (2004) and Pedro & Kobayasaki (2004) and Johari (2007) and Custodio (2008). The reason for higher lift to drag ratios was attributed to the flow remaining attached to the hydrofoil for a larger period and therefore, delaying stall. The studies also showed that the higher lift to drag ratio can be supported by the geometry of the hydrofoils and the variation of the velocity and pressure gradient in trough area causing the increase of the streamwise vorticity strength that exists in counter rotating formations in a number that is related to the number of the tubercles. This was observed by the research performed by Hansen et al (2011) and Stanway (2008). The vorticity strength stretched, tilted and diffused in three dimensions and the interaction with the boundary layer contributing to the momentum exchange remains the main argument that this hydrofoils maintain higher lift to drag ratios for high angle of attacks. The advantage of these hydrofoils in maintaining the lift under stall conditions has motivated the research for applying these hydrofoils in tidal turbines. Weichao Shi et al (2017) have conducted and presented experimental and computational results for various designs of tidal turbines proving that turbines with tubercles could under certain conditions improve the hydrodynamic performance of these turbines. The hydrodynamic characteristics of hydrofoils with tubercles deserves to be fully explored and their behaviour under cavitation needs to be further studied and understood. Furthermore, it is important to understand the three dimensional effects of these hydrofoils and to investigate their application to more complex geometries like for marine propellers. To determine whether cavitation can be reduced by using propellers with tubercles is also important since this could contribute to the reduction of the underwater acoustic footprint by applying this design concept.

2 NUMERICAL MODEL

This paper analyses the effect of the tubercles for the

DTMB 4119 propeller. The geometric characteristics of this propeller without tubercles can be seen in table 1. This propeller has diameter of $D = 0.3048m$, three blades and a variable pitch.

The propeller has been experimentally tested and the thrust K_T, torque coefficient K_Q and its efficient η are known for different advance ratios J. In this section the methodology and the tools that have been utilized are provided. The detailed geometry generation, the mesh generation and the development of a mesh that would give a mesh independent solution are provided.

Table 1: Geometry of the propeller

rR	cD	PD	Tc	Fc
0.2	0.32	1.1050	0.2055	0.01429
0.3	0.3625	1.1020	0.15530	0.02318
0.4	0.4048	1.0980	0.11800	0.02303
0.5	0.4392	1.0930	0.09160	0.02182
0.6	0.4610	1.0880	0.06960	0.02072
0.7	0.4622	1.0840	0.05418	0.02003
0.8	0.4347	1.0810	0.04206	0.01967
0.9	0.3613	1.0790	0.03321	0.01817
0.95	02775	1.0770	0.03228	0.01631
1	0.000	1.0750	0.03160	0.01175

2.1 Propeller geometry

The geometry of the propeller has be generated using OpenProp. With OpenProp the section foil profiles and the guide curves have been generated and then they have been imported to a CAD software in order to create the solid model of the propeller without the tubercles. For the propeller with tubercles a subroutine has been added to OpenProp in order to generate the sinusoidal shape of the propeller leading edge. In this paper only the effect of a single tubercle is presented, aiming to identify the three dimensional hydrodynamic effects of the tubercles for a skewed propeller. The difference in comparison to the hydrofoils with tubercles is that the sinusoidal profile needs to geometrically follow the blades reference line and this involves an increased complexity in terms of generating a propeller geometry with tubercles that will follow the expression in 1 as proposed by Johari (2018). The geometry is characterized by c_z, the local chord length of the hydrofoil, z the spanwise coordinate, A the amplitude of the hydrofoil and λ the wave length. For the propeller blade expression 1 needs to be applied in smaller sections along the blade reference line. In figures 1 and 2 the solid geometry of the propeller with tubercles and without tubercles is presented.

$$c_z = c + Asin\Big(\frac{2\pi z}{\lambda} - \frac{\pi}{2}\Big). \quad (1)$$

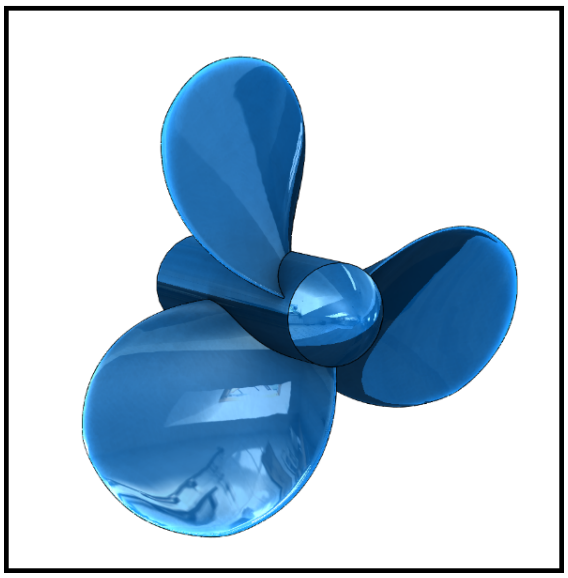

Figure 1: The 3-D solid model of the DTMB 4119 propeller.

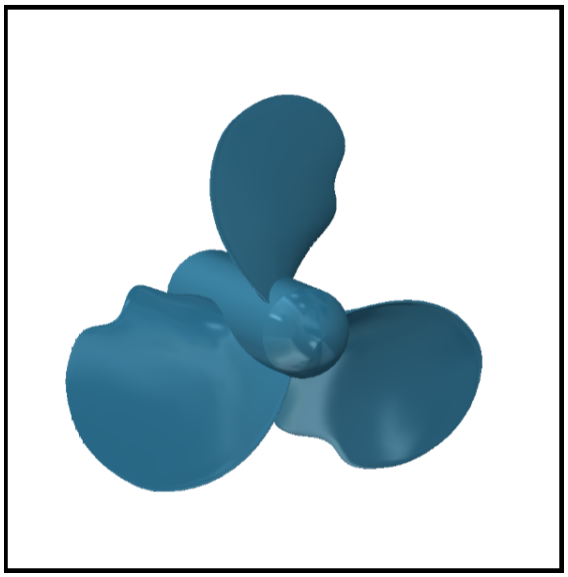

Figure 2: The 3-D solid model of the modified DTMB 4119 propeller.

2.2 Mesh specification and boundary conditions

Two separate domains have been meshed, a cylindrical domain similar with the computational domain used by Lloyd et.al (2017) with an upstream length of $2.8D$ and downstream length $7.4D$ shown in figure 3 which presents the two merged domains. The mesh generated is a tetrahedral mesh with an inflated quad mesh on the propeller surface for an initial thickness to satisfy $y^+ < 30$.

The final study of the mesh that has been generated after a mesh sensitivity analysis performed, is presented in 3. The mesh for the cylindrical domain consists from 8 million elements and for the propeller domain from 4 million elements. In figure 4 the mesh for the cylindrical domain is presented and the mesh for the propeller is presented in 5.

In order to take into account the rotation of the propeller, an interphase is created between the stationary cylindrical part and the propeller. The model interphase can be used for a steady state and transient solution producing accurate results in cases where the circumferential variation of the flow is higher relative to the component pitch. Furthermore, this interphase model can reduce the computational requirements of the simulation.

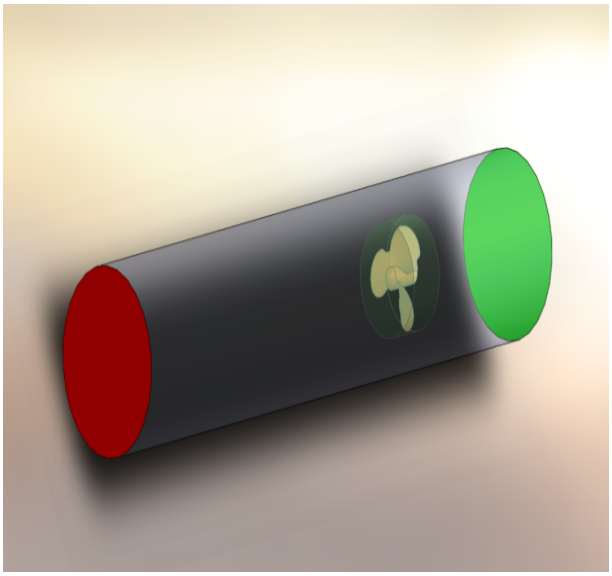

Figure 3: Computational domain.

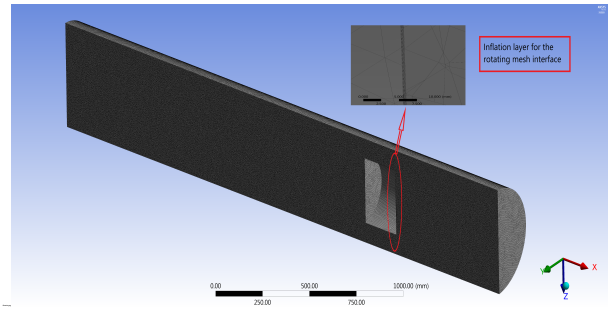

Figure 4: Mesh for the cylindrical domain.

A summary of the operational conditions and the boundary conditions simulated for the propeller with tuburcles and without tubercles are shown in tables 2 and 3. The operational conditions were chosen taken into account the availability of experimental results for the DTMB 4119 propeller. Therefore, the CFD simulations performed for two different advance coefficients and with a constant cavitation number, that was used to calculate the static pressure at the outlet boundary condition.

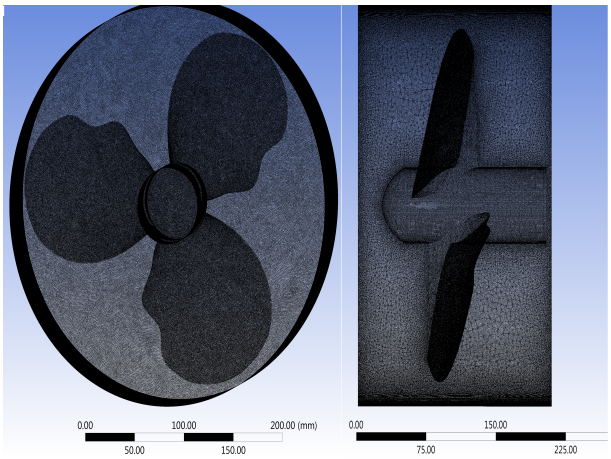

Figure 5: Mesh for the propeller

Table 2: Operational conditions

No	J	cavitation number σ	Vinlet	n (rev/s)
1	0.88	2.5	2	6.530
2	1.0	2.5	2	5.747

A constant velocity normal to the inlet boundary condition has been applied in the cylindrical domain and a constant static pressure in the outlet boundary condition. The boundary condition for the propeller region has been set as non-slip wall and the cylindrical domain as slip wall.

Table 3: Boundary conditions

Boundary	**Velocity**	**Pressure**	**Vapour fraction**
Inlet	Fixed	zero gradient	0
Outlet	Zero gradient	Fixed	0
Propeller	No-Slip	Zero gradient	Wall model applied
Cylindrical domain	Slip	Zero gradient	Zero gradient

2.3 Turbulence model

The aim of this work is to model a cavitating flow which is non-Boussinesq and compressible flow using CFD methods in order to solve the Reynolds averaged Navier-Stokes equations. Therefore, the use of a turbulence model is required. Furthermore, turbulence in the vapour phase has an influence on the overall dynamics of cavitation modelling. The dynamics are controlled by the changing inertia of the fluid mixture, and the turbulence and vorticity generated at the walls. Therefore, it is important to resolve the turbulence structures with accuracy. One of the most popular turbulence model used for similar applications due to the advantage in resolving very well the near wall law resolution is the k- ω SST model which also requires relatively low computational time. One of the advantage of this model is that it can combine the Wilcox model near the wall

and the k-ϵ model for the flow away from the wall. Following the governing equations according to the ANSYS CFX: Turbulence kinetic energy:

$$\frac{\partial k}{\partial t}+U_j\frac{\partial k}{\partial x_j}=P_k-\beta^{'}\rho k\omega+\frac{\partial}{\partial x_j}\big[(\nu+\sigma_k v_T)\frac{\partial k}{\partial x_j}\big]. \quad (2)$$

Specific dissipation rate ω:

$$\frac{\partial(\rho\omega)}{\partial t}+\frac{\partial(\rho U_j\omega)}{\partial x_j}=\frac{\partial}{\partial x_j}\big[(\mu+\frac{\mu_\tau}{\sigma_\omega})\frac{\partial\omega}{x_j}\big]+\alpha\frac{\omega}{k}P_k-\beta\rho\omega^2 + P_{\omega b}. \quad (3)$$

Where ρ is density, $\mathbf{U}$ the velocity vector, P_k is the production rate of turbulence, β, α, β', σ_k and σ_ω are the model constraints, and their values can be found in the manual. The k-ω SST model is accurate in the prediction of flow separation in surfaces and this is because the SST model uses a different formulation of the eddy viscosity formulated as:

$$\nu_t=\frac{a_1 k}{max(a_1,\omega,SF_2)}, \quad (4)$$

where F_2 is a blending function which restricts the limiter to the wall boundary layer and S is an invariant measure of the strain rate. More detail on these functions can be found in the ANSYS CFX manual.

2.4 Cavitation model

A two phase CFD model is used that consists of two phases: one liquid (water) and one vapour phase. As a result the RANS equations are solved for a mixture fluid with a density ρ_m, the density is calculated in the flow cells provided that the volume fractions between the two phases are known. The cavitation model used for this case is a simplified Rayleigh-Plesset model that ignores the gas dissolved in water the viscosity stresses due to the enclosed liquid, vapour and gas that are moving in a radial direction inside a formed bubble.

$$R_B\frac{dR_B^2}{dt^2}+\frac{3}{2}\Big(\frac{dR_B}{dt}\Big)^2+\frac{2\sigma}{\rho_f R_B}=\frac{p_v-p}{\rho_f}, \quad (5)$$

where R_B is the bubble radius, p_v the vapour pressure at the liquid temperature, p is the pressure surrounding the bubble, ρ_f the water density at constant pressure and σ is the surface tension coefficient between the liquid and the vapour. Furthermore, this equation reduces to (6), since the surface tension and the second order terms are ignored from (5):

$$\frac{dR_B}{dt}=\sqrt{\frac{2}{3}\frac{p_v-p}{\rho_f}}, \quad (6)$$

The rate of change of the bubble mass will then become:

$$\frac{dm_B}{dt}=\rho_g\frac{dV_B}{dt}=4\pi R_B^2\rho_g\sqrt{\frac{2}{3}\frac{p_v-p}{\rho_f}}. \quad (7)$$

where, ρ_g is the density of the bubble content, V_B is the volume of a individual bubble and R_B is the bubble radius. In order to identify the total interphase mass transfer rate per unit volume of the bubbles the volume fraction r_g is expressed as:

$$r_g=V_B N_B=\frac{4}{3}\pi R_B^3 N_B, \quad (8)$$

This results to the total interphase rate per unit volume to be expressed as:

$$\dot{m}_{fg}=N_B\frac{dm_B}{dt}=\frac{3r_g\rho_g}{R_B}\sqrt{\frac{2}{3}\frac{p_v-p}{\rho_f}}. \quad (9)$$

In order to generalize equation (9) the software uses the empirical factor F that differs for condensation and vaporization, in order to take into account the different rates of the two phenomena therefore, (9) becomes :

$$\dot{m}_{fg}=F\frac{3r_g\rho_g}{R_B}\sqrt{\frac{2}{3}\frac{|p_v-p|}{\rho_f}}sgn(p_v-p), \quad (10)$$

Furthermore, for modelling purposes the bubble radius R_B is replaced by the nucleation radius R_{nuc}. The vaporization is initiated at nucleation regions where the water tensile strength is reduced. These sites can be regions where an increased volumetric concentration of non-condensible gases are present and can act as cavitation generators. Therefore, the model can take into account the possible cavitation sides and this is resulting to increased volume fractions and as a result the finite number of the nucleation sites has to be decreased accordingly because the liquid volume is also decreased. The vaporization fraction r_g is replaced to the nucleation fraction $r_{nuc}(1-r_g)$ and (9) is becoming:

$$\dot{m}_f g=F\frac{3r_{nuc}(1-r_g)\rho_g}{R_{nuc}}\sqrt{\frac{2}{3}\frac{|p_v-p|}{\rho_f}}sgn(p_v-p). \quad (11)$$

Where r_{nuc} is the volume fraction of the nucleation sites. The calculation of the mass transfer rate, requires the assumption of the model parameters and the default values in the software are set as following:

a) $R_{nuc}=1\mu m$

b) $r_{nuc}=5\times10^{-4}$

c) $F_{vap}=50$

d) $F_{cond}=0.01$

3 RESULTS FROM THE PROPELLER ANALYSIS

The performance coefficient have been used to calculate both the propellers with and without tubercles. These coefficients are summarized as follows:

$$K_T = \frac{T}{\rho_f n^2 D^4} \qquad K_Q = \frac{Q}{\rho_f n^2 D^5}$$
$$\eta = \frac{K_T J}{2\pi K_Q} \qquad J = \frac{U}{nD}.$$

Where, K_T is the thrust coefficient, T the thrust. K_Q is the torque coefficient and Q the torque, η is the open water efficiency of the propeller. In table 4 the computational results for the two advance ratios are presented. The performance coefficients have been calculated for wetted steady state simulations and have been evaluated using the experimental results from the open water tests performed and can be seen in figure 6. The experimental results available are for the propeller without tubercles, since for the propeller with the tuburcles has not been tested experimentally. Comparing the computational results with the experimental results there is a difference for both the advance ratios used in the calculations that is close to 10 %. Furthermore, the propeller with tubercles have higher coefficient numbers for both cases that have been calculated therefore, further study of these hydrofoils could be beneficial in terms of understanding the propeller performance.

Table 4: Propeller coefficients for tubercles and without tubercles

With Tubercles			
J	K_T	$10K_Q$	η
0.88	0.0811	0.241	0.467
1.0	0.005877	0.134	0.685
Without Tubercles			
J	K_T	$10K_Q$	η
0.88	0.0763	0.229	0.459
1.0	0.0529	0.117	0.706

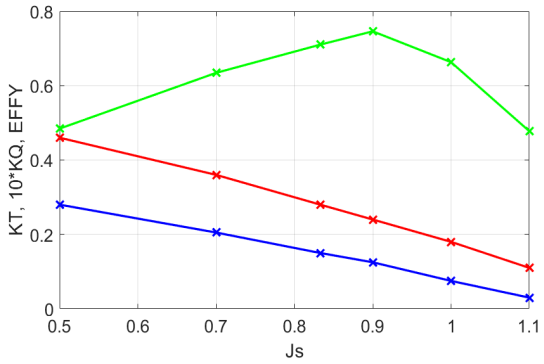

Figure 6: Experimental results for the Propeller DTMB 4119

4 INFLUENCE OF CAVITATION ON SIMPLE PROPELLER

The pressure distribution in the suction and pressure sides of the propeller are presented in figure 7 for two advance ratios. The areas with lower pressure are close to the hub of the propeller. For an advance ratio $J = 1$ the low pressure region is extended up to 40 % in the spanwise direction, this can be an indication of having cavitation inception in these low pressure regions.

The distribution of cavitation can be seen in figure 8 for different blade positions starting from 0^o to 279^o. The iso-surface presents in this figures the vapour volume fraction of 10 % that is applied to the blade surface domain. For both cases studied sheet type cavitation was most frequently predicted in the suction side of the propeller close to the hub. For some cases however, bubble cavitation is possible even though the model that is used cannot directly capture the development of individual or isolated bubbles. However, the concentration of the vapour volume ratio in these areas observed is very small that can be interpreted as bubble type cavitation. This is most frequently observed for the advance ratio of $J = 0.88$. As it was expected lower cavitation is present for the advance ratio of $J = 0.88$ since this point is close to the design point of the propeller. For the advance ratio of $J = 1$ cavitation predicted seems to be persistent close to the hub region and it starts to fade off after the blade position reaches 103^o. It needs to be said that for the transient calculations the simulations were performed for a time period to allow the numerical instabilities present in the beginning of the simulation to reduce. Therefore, the simulation performed for a time period corresponding to 10 rotation cycles.

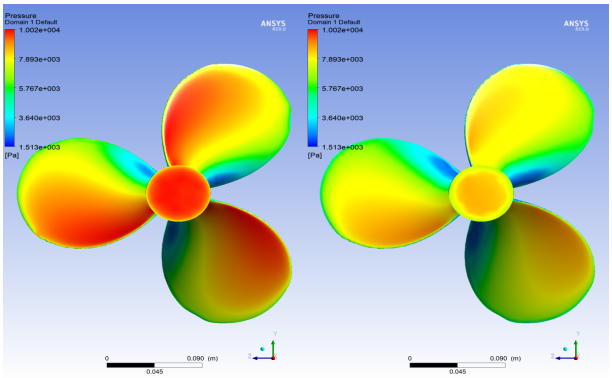

(a) Pressure distribution at the pressure surface of the propeller J=0.88 and J=1 respecitvely.

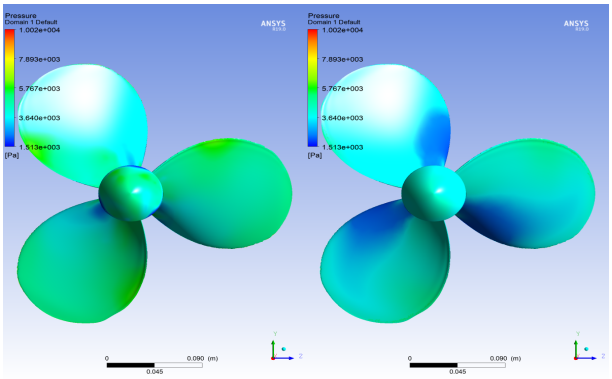

(b) Pressure distribution at the suction surface of the propeller J=0.88 and J=1 respecitvely.

Figure 7: Comparison of pressure distribution for different advance ratios

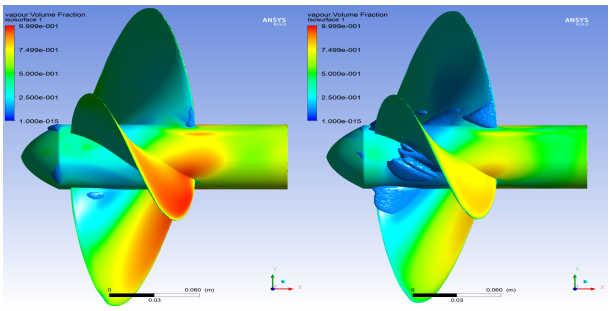

(a) Propeller side view of the iso-surface of 10 % vapour volume for J=0.88 and J=1 at a blade angle 0^o.

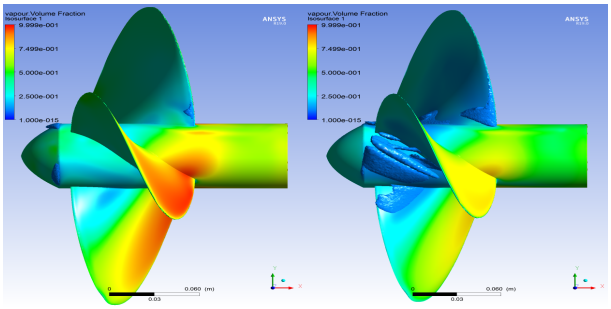

(b) Propeller side view of the iso-surface of 10 % vapour volume for J=0.88 and J=1 at a blade angle 45^o.

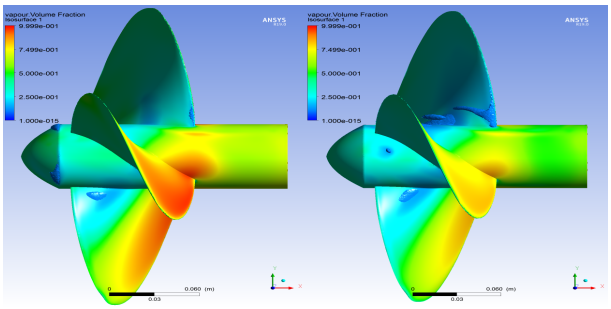

(c) Propeller side view of the iso-surface of 10 % vapour volume for J=0.88 and J=1 at a blade angle of 103^o.

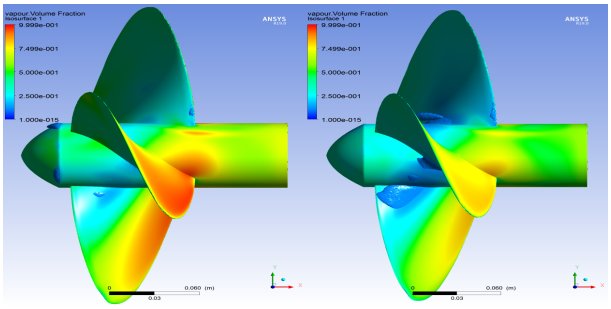

(d) Propeller side view of the iso-surface of 10 % vapour volume for J=0.88 and J=1 at a blade angle 161^o.

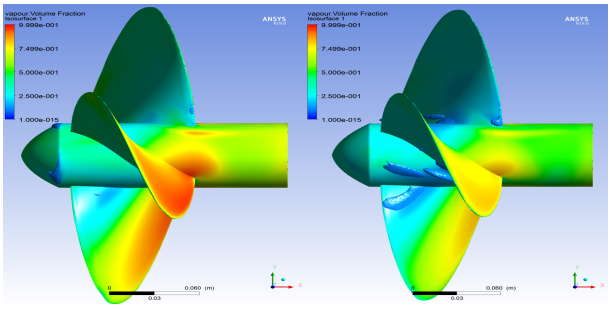

(e) Propeller side view of the iso-surface of 10 % vapour volume for J=0.88 and J=1 at a blade angle 279^o.

Figure 8: Comparison of cavitation distribution for different advance ratios and different propeller blade positions.

5 INFLUENCE OF TUBERCLES ON A PROPELLER WITHOUT CAVITATION

In order to study the influence of the tubercles a wetted steady state simulation has been performed for the propeller with tubercles. It is known that the positive hydrodynamic effects of the tubercles are mainly attributed to the high streamwise vorticity that is generated by the tubercles and the possible prolonged flow attached to the blade surface before the flow separation at high angle of attacks ($> 20^o$). Furthermore, at the post-stall region these hydrofoils retain a higher pressure coefficient and also a higher lift to drag ratio, giving them an advantage in comparisson to the hydrofoil with a straight leading edge geometry. In this case, the vorticity has been calculated for both propellers and the results are presented in figure 9, and show that the total vorticity is higher close to the trough region of the tubercle. However, the strength of the total vorticity does not extend in the stream wise direction as it is usually the case with the hydrofoil which could be the result of the tubercle geometry chosen for this study combined with the rotation of the propeller and the hydrodynamic effects incorporated by the rotation.

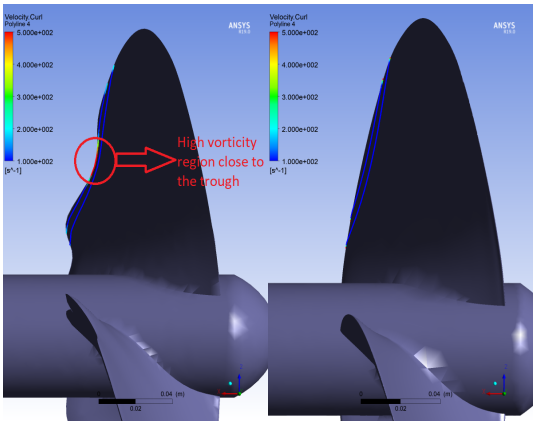

(a) Vorticity at the propeller pressure side surface.

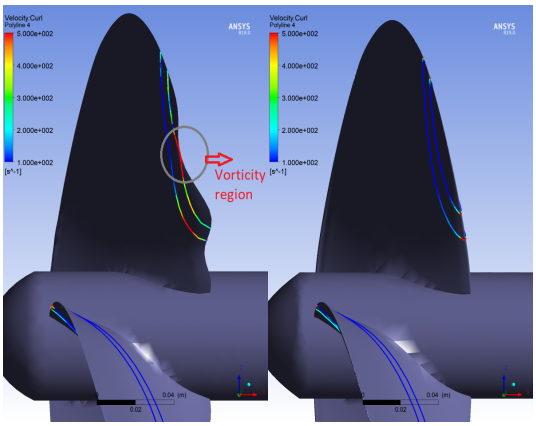

(b) Vorticity at the propeller suction side surface.

Figure 9: Comparison of vorticity for propeller different geometries.

Additionally, the results for the pressure coefficient that were calculated for the normalized X and Y direction are

presented in 10. As it can be seen, the most negative values of the pressure coefficient that are developed at the suction surface can be attributed to the effect of the trough in this region. Furthermore, lower negative values compared to the propeller without tubercles can also be seen close to the tubercles peak area.

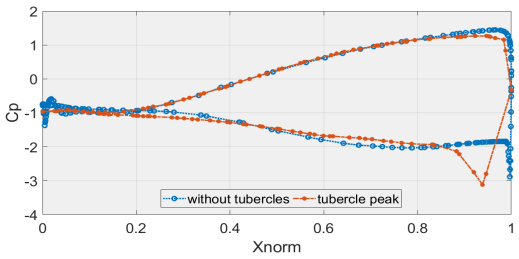

(a) Pressure coefficent at the normalized X direction.

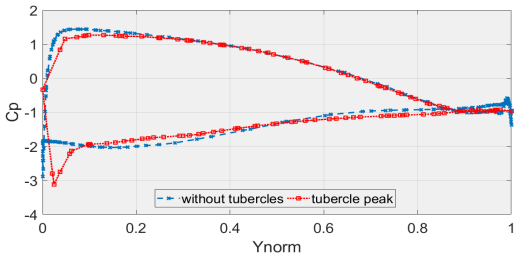

(b) Pressure coefficent distribution at the normalized Y direction.

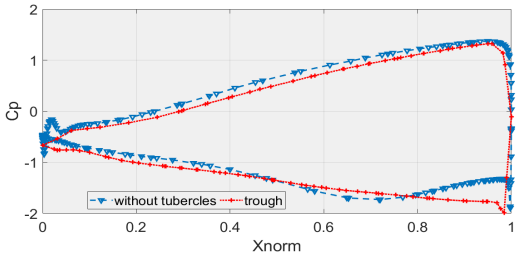

(c) Pressure coefficent distribution at the normalized X direction.

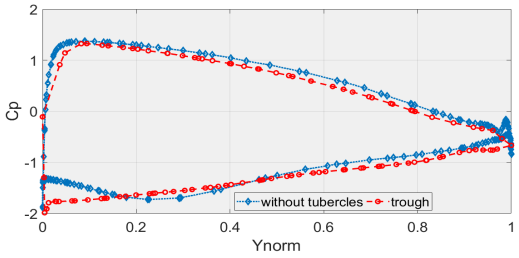

(d) Pressure coefficent distribution at the normalized Y direction.

Figure 10: Comparison of the pressure coefficient distribution for a propeller with tubercles and without tubercles.

6 INFLUENCE OF CAVITATION ON PROPELLER WITH TUBERCLES

In the final section the results of the propeller with tubercles including the calculations for predicting cavitation are evaluated. In figure 11 the isosurface presenting 10 % of the vapour volume fraction is presented for a propeller with an advance ratio of $J = 0.88$. In both these regions cavitation is present. However, it can be seen that the cavitation is isolated only on these two areas and is not extended in the spanwise direction of the leading edge. This compartmentalization of the cavitation is easier to control by altering the tubercles geometry. This needs to be further studied and evaluated.

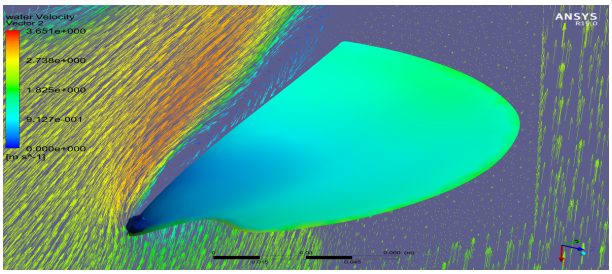

(a) Isosurface 10 % volume vapour fraction to peak of tubercle at a blade position of 90^o.

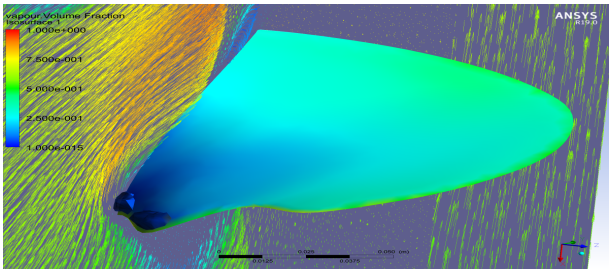

(b) Isosurface 10 % volume vapour fraction to trough of tubercle at a blade position of 90^o.

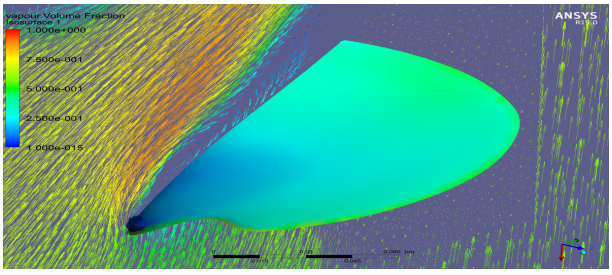

(c) Isosurface 10 % volume vapour fraction to peak of tubercle at a blade position of 360^o.

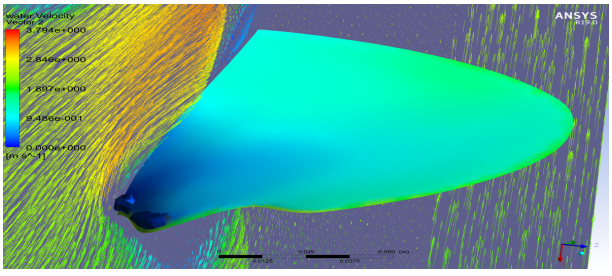

(d) Isosurface 10 % volume vapour fraction to trough of tubercle at a blade position of 360^o.

Figure 11: Isosurfaces of 10 % volume vapour fraction for different blade positions and.

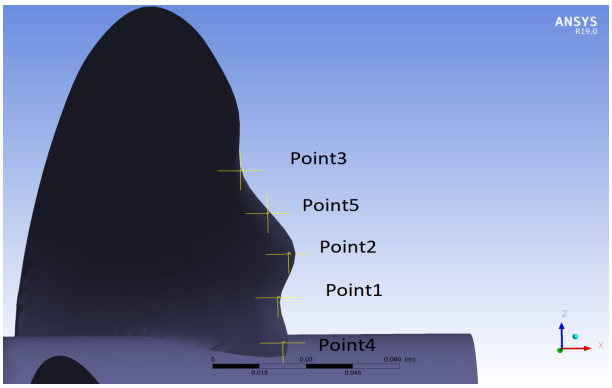

Figure 12: Points for the transient cavitation calculations

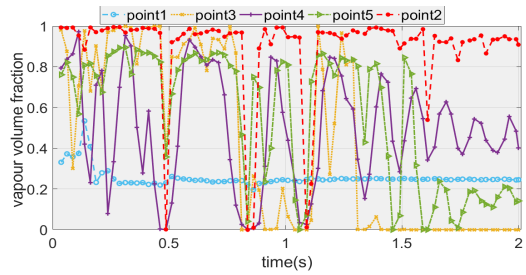

(a) Volume vapour fraction at the propeller leading edge for advance ratio $J = 1$.

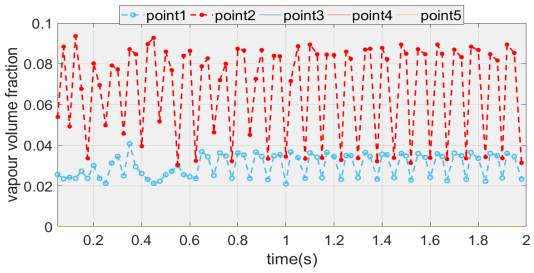

(b) Volume vapour at the propeller leading edge for advance ratio of $J = 0.88$.

Figure 13: Transient values for the vapour fraction for different advance ratios.

Finally figure 12 shows the points where results from the transient calculations for the cavitation volume fraction have been taken and presented in figures 13a and 13b. The simulation has predicted that the cavitation is higher for the advance ratio $J = 1$ and also more persistent compared to the advance ratio $J = 0.88$. Furthermore, the behaviour for the $J = 1$ case is worst compared to the cavitation predicted for the propeller without tubercles. This shows that the alteration of the leading edge geometry needs to be done with caution taking into account advance ratios that are outside the optimum design point.

CONCLUSIONS

Tubercles could be used to control sheet cavitation and under specific operational conditions could increase the propeller performance. However, applying the tubercles in the propeller needs to be performed with caution since they can deteriorate the performance of the propeller especially in cases it operates outside the optimum design envelope. For these cases cavitation can be severe and compromise the performance of the propeller significantly and increase the generated noise. Further optimization and study is required with regards to the geometry of the tubercles and for controlling cavitation for a number of operational conditions.

REFERENCES

Watts, P. , Fish, F.E. (2001). 'The influence of passive, leading edge tubercles on wing performance.' In Proceedings of the Twelfth International Symposium on Unmanned Untethered Submersible Technology UUST, Lee, NH. Auton. Undersea Syst. Inst.

Miklosovic, D. S., Murray, M.M., Howle, L.E. & Fish, F.E. (2004). 'Leading-edge tubercles delay stall on humpback whale (Megaptera novaeangliae) flippers.' Physics of Fluids 16 L.39

Pedro, H.T. C.,& Kobayashi, M.H. (2008) 'Numerical study of stall delay on humpback whale flippers.' 46th AIAA Aerospace Sciences Meeting and Exhibit, Reno, Nevada.

Johari, H. & Henoch, C.W., Custodio, D. & Levshin, A. (2007). 'Effects of leading-edge protuberances on airfoil performance.'. AIAA J. 45 2634–2642.

Custodio, D. (2007). 'The effect of Humpback Whale-Like Leading Edge Protuberances on Hydrofoil Performance'. Worcester Polytechnic Institute.

Stanway, M J., (2008). 'Hydrodynamic effects of leading edge tubercles on control surfaces and in flapping foil propulsion'. Masters, Massachusetts Institute of Technology.

Hansen, K. L., Rostamzadeh, N.,Kelso, R. M. & Dally, B. (2016). 'Evolution of the streamwise vortices generated between leading edge tubercles.' Journal Fluid Mechanics vol. 788, pp. 730-766.

Weichao S., Atlar M., Norman R.(2017) 'Humpback whale inspired design for tidal turbine blades'.Fifth International Symposium on Marine Propulsors., Espoo, Finland.

Lloyd T.,Vaz G., Rijpkema, D., Reverberi, A. (2017) 'Computational fluid dynamics prediction of marine propeller cavitation including solution verification' Fifth International Symposium on Marine Propulsors., Espoo, Finland.

Johari, H. (2015) 'Cavitation on hydrofoils with sinusoidal leading edge' 9th International Symposium on Cavitation (CAV2015), EPFL, Lausanne, Switzerland

ANSYS, (2014). 'Solver Theory Guide CFX 19.0'. ANSYS-CFX, Pennsylvania', USA.